

# Lithium abundance in lower red giant branch stars of Omega Centauri <sup>★</sup>

A. Mucciarelli<sup>1,2</sup>, M. Salaris<sup>3</sup>, L. Monaco<sup>4</sup>, P. Bonifacio<sup>5</sup>, X. Fu<sup>1,2</sup>, S. Villanova<sup>6</sup>

<sup>1</sup> Dipartimento di Fisica e Astronomia, Università degli Studi di Bologna, Via Gobetti 93/2, I-40129 Bologna, Italy;

<sup>2</sup> INAF - Osservatorio di Astrofisica e Scienza dello Spazio di Bologna, Via Gobetti 93/3, I-40129 Bologna, Italy;

<sup>3</sup> Astrophysics Research Institute, Liverpool John Moores University, 146 Brownlow Hill, Liverpool L3 5RF, United Kingdom

<sup>4</sup> Departamento de Ciencias Físicas, Universidad Andres Bello, Fernandez Concha 700, Las Condes, Santiago, Chile

<sup>5</sup> GEPI, Observatoire de Paris, Université PSL, CNRS, Place Jule Janssen 92190, Meudon, France

<sup>6</sup> Universidad de Concepción, Casilla 160-C, Concepción, Chile

Preprint online version: July 23, 2018

## ABSTRACT

We present Li, Na, Al and Fe abundances of 199 lower red giant branch stars members of the stellar system Omega Centauri, using high-resolution spectra acquired with FLAMES at the Very Large Telescope. The A(Li) distribution is peaked at A(Li)~1 dex with a prominent tail toward lower values. The peak of the distribution well agrees with the lithium abundances measured in lower red giant branch stars in globular clusters and Galactic field stars. Stars with A(Li)~1 dex are found at metallicities lower than [Fe/H]~-1.3 dex but they disappear at higher metallicities. On the other hand, Li-poor stars are found at all the metallicities. The most metal-poor stars exhibit a clear Li-Na anticorrelation, with about 30% of the sample with A(Li) lower than ~0.8 dex, while in normal globular clusters these stars represent a small fraction. Most of the stars with [Fe/H]>-1.6 dex are Li-poor and Na-rich. The Li depletion measured in these stars is not observed in globular clusters with similar metallicities and we demonstrate that it is not caused by the proposed helium enhancements and/or young ages. Hence, these stars formed from a gas already depleted in lithium. Finally, we note that Omega Centauri includes all the populations (Li-normal/Na-normal, Li-normal/Na-rich and Li-poor/Na-rich stars) observed, to a lesser extent, in mono-metallic GCs.

**Key words.** stars: abundances – stars: atmospheres – stars: evolution – stars: Population II – (Galaxy:) globular clusters: individual (Omega Centauri)

## 1. Introduction

The emergent and generally accepted picture of stellar populations in globular clusters (GCs) is that these stellar systems host different (chemically distinct) stellar populations. In the majority of the cases, the stars of a GC share the same abundances of most of the elements, in particular Fe and iron-peak elements (see e.g. Carretta et al. 2009c; Willman & Strader 2012) demonstrating that these systems are not able to retain the ejecta of the supernovae. On the other hand, light elements (C, N, O, Na, Mg and Al) exhibit large star-to-star variations and often coherent patterns, i.e. C-N, Na-O and Mg-Al anti-correlations (see e.g. Smith & Norris 1982; Kraft et al. 1992; Carretta et al. 2009a,b; Gratton, Carretta & Bragaglia 2012; Meszaros et al. 2015; Pancino et al. 2017; Bastian & Lardo 2017). These chemical patterns are usually interpreted as the signature of internal pollution by low-energy ejecta of stars where high-temperature proton-capture cycles (CNO, NeNa and MgAl cycles) occurred. The so-called first population (1P) of the cluster is composed by stars with the same chemical composition of the original cloud from which the cluster formed. Instead, the subsequent second populations (2P) stars show variations of the light element abundances and they are expected to form from the pristine gas diluted with the ejecta of the polluter stars. A complete and quanti-

tatively successful model for this self-enrichment process is still lacking, being several details still debated (see e.g. Renzini et al. 2015; Bastian & Lardo 2015), for instance the identification of the main polluter stars. Most favorite candidate polluter stars are asymptotic giant branch (AGB) stars with masses of 4–8  $M_{\odot}$  (Ventura et al. 2001; D’Ercole et al. 2008, 2010) and fast rotating massive stars (Meynet, Ekström & Maeder 2006; Prantzos & Charbonnel 2006; Decressin et al. 2007).

The abundance of lithium – A(Li)<sup>1</sup> – in GC stars is a valuable diagnostic to understand this self-enrichment process, that poses challenges to the current theoretical models for the formation/evolution of GCs. Lithium is one of the few elements created during the Big Bang nucleosynthesis, together with H and He. In the subsequent evolution of the stars, Li is destroyed in the stellar interiors due to proton capture reactions occurring at  $\sim 2.5 \cdot 10^6$  K. However, Li should be preserved in the stellar envelopes of unevolved stars or partially diluted in the photospheres of the stars that have undergone processes of mixing. The main mixing episodes are the first dredge-up (FDU) after the completion of the main sequence stage, and the extra-mixing episode occurring at the luminosity level of the red giant branch (RGB) bump. Because the proton-capture reactions responsible for the chemical anomalies observed in GC stars occurred at temperatures significantly higher ( $> 10^7$  K) than that of the Li-burning ( $\sim 10^6$  K), the enriched material from which the 2P stars

Send offprint requests to: A. Mucciarelli

<sup>★</sup> Based on observations collected at the ESO-VLT under program 096.D-0728.

<sup>1</sup>  $A(\text{Li}) = \log \frac{n(\text{Li})}{n(\text{H})} + 12.00$

formed should be Li-free. Therefore, a Li-Na anticorrelation and a Li-O correlation are expected within the individual clusters.

Abundances of Li in GCs have been obtained from dwarf and lower RGB (LRGB) stars. The latter are stars located between the FDU and the RGB bump. Even if measures of  $A(\text{Li})$  are limited to a few GCs, the emerging scenario turns out to be complex, with some GCs showing evidence of star-to-star scatter in  $A(\text{Li})$ , like in the cases of NGC 6397 (Lind et al. 2009; Gonzalez Hernandez et al. 2009), NGC 6752 (Pasquini et al. 2005; Shen et al. 2010), M4 (Monaco et al. 2012), NGC 2808 (D’Orazi et al. 2015) and 47 Tucanae (D’Orazi et al. 2010; Dobrovolskas et al. 2014). Other clusters (M92, NGC 362, NGC 1904, NGC5904 and NGC 6218, Bonifacio 2002; D’Orazi et al. 2014, 2015) show a remarkably homogeneous Li abundance. Up to now the only clusters that exhibit undeniable evidence of correlations between Li and light-elements are NGC 6752 that shows both Li-O correlation (Shen et al. 2010) and Li-Na anticorrelation (Pasquini et al. 2005), NGC 6397 where 3 Li-poor, Na-rich dwarf stars have been found (Lind et al. 2009) and NGC 2808, where some Al-rich RGB stars have  $A(\text{Li})$  lower than that in other stars with similar Al content (D’Orazi et al. 2015). In M4 a hint of Li-Na anticorrelation is found (Monaco et al. 2012), with a larger  $A(\text{Li})$  scatter among 2P stars with respect to 1P stars but no evidence of Li-O correlation (Mucciarelli et al. 2011). 47 Tucanae shows the opposite situation, with a statistically significant Li-O correlation but not clear evidence of a Li-Na anticorrelation (Dobrovolskas et al. 2014).

In this paper we investigate the Li content in the stellar system Omega Centauri (NGC 5139) using LRGB stars, with the final aim to highlight possible correlations with abundances of light elements involved in the chemical anomalies. Traditionally classified as a GC, Omega Centauri exhibits (at variance with the other globulars) a wide iron distribution (Johnson et al. 2008, 2009; Johnson & Pilachowski 2010; Villanova et al. 2014; Pancino et al. 2011a; Marino et al. 2011) and a variety of discrete sub-sequences in its colour-magnitude diagram (CMD, Lee et al. 1999; Pancino et al. 2000; Ferraro et al. 2004; Bedin et al. 2004; Sollima et al. 2005a, 2007; Milone et al. 2008), suggesting that this system has been able to retain the ejecta of the supernovae, experiencing a chemical enrichment history more complex than that of a normal GC. According to this evidence, Omega Centauri is usually interpreted as the remnant of a disrupted dwarf spheroidal galaxy (Bekki & Freeman 2003). On the other hand, its dominant (metal-poor) population shows a clear Na-O anticorrelation (Johnson & Pilachowski 2010; Marino et al. 2011), demonstrating that the same self-enrichment process observed in mono-metallic GCs occurred also in this stellar system.

The only determination of  $A(\text{Li})$  in Omega Centauri stars has been presented by Monaco et al. (2010) who analysed a sample of 91 dwarf stars in the iron range  $[\text{Fe}/\text{H}] = -2.0/-1.4$  dex, finding an average lithium  $A(\text{Li}) = 2.19$  dex ( $\sigma = 0.14$  dex). This abundance is compatible with the values usually measured among the Galactic dwarf stars. Measures for light element abundances are not available for this sample of dwarf stars. Because of the faintness of the dwarf stars in Omega Centauri ( $V > 18$ ), large samples of high quality spectra can be obtained only with a huge effort in terms of telescope time. The observation of LRGB stars (instead of dwarf stars) allows to study the lithium content in Omega Centauri using large sample of high signal-to-noise (SNR), high-resolution spectra, coupling these abundances with those of the light elements in order to study the lithium content in 1P and 2P stars.

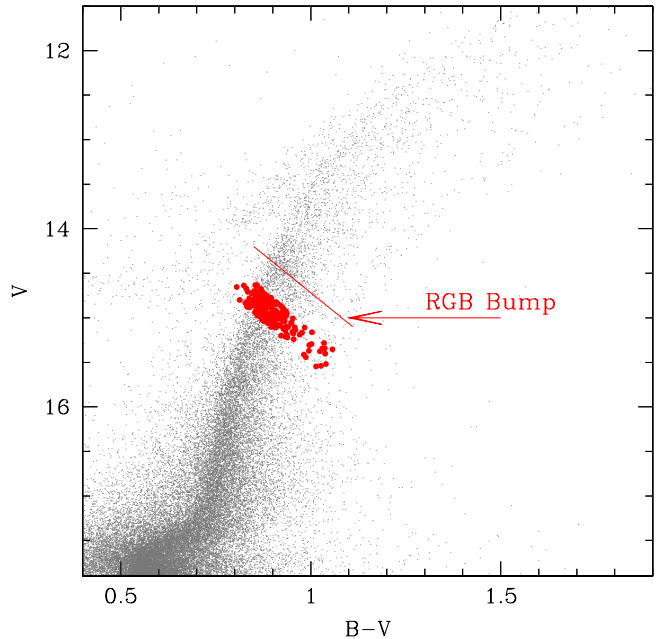


**Fig. 1.** CMD of Omega Centauri (Bellini et al. 2009, stars selected within 750 arcsec from the cluster center), with marked the position of the spectroscopic targets (red circles) and the mean locus (red line) of the RGB bump of the different stellar populations of Omega Centauri.

The paper is structured as follows: Section 2 describes the observations and selection of the member stars of Omega Centauri; Section 3 describes the adopted procedure for the chemical analysis; the results are presented in Section 4, 5 and 6 and discussed in Section 7.

## 2. Observations and membership

The observations have been collected under the ESO program 096.D-0728 (PI: Mucciarelli) using the multi-object spectrograph FLAMES (Pasquini et al. 2000) at the Very Large Telescope. The GIRAFFE+UVES combined mode has been used, allowing the simultaneous allocation of 132 mid-resolution GIRAFFE fibers and 8 high-resolution UVES (Dekker et al. 2000) fibers.

All the stars have been observed with three FLAMES-GIRAFFE set-ups, namely HR12 ( $\Delta\lambda = 5821-6146 \text{ \AA}$ ,  $R \sim 20000$ ), HR13 ( $\Delta\lambda = 6120-6405 \text{ \AA}$ ,  $R \sim 26000$ ) and HR15N ( $\Delta\lambda = 6470-6790 \text{ \AA}$ ,  $R \sim 19000$ ), allowing the measure of several Fe spectral lines, as well as the Li line at  $6708 \text{ \AA}$ , the Na D doublet at  $5890-5896 \text{ \AA}$  and the Al I doublet at  $6696-6698 \text{ \AA}$ . Two observations of 1350 s each have been secured for HR12, 4 exposures of 1800 s each for HR12 and 6 exposures of 2700 s each for HR15N. Two target configurations have been taken, observing a total of 211 stars.

The targets have been selected from the Bellini et al. (2009) BVRI WF12.2m photometric catalogue, picking stars  $\sim 0.6$  mag fainter than the mean locus of the RGB bump. These stars are hence located after the completion of the FDU and before the onset of the extra-mixing usually observed after the RGB bump. Fig. 1 shows the positions of the observed targets (red circles), together with the mean locus of the RGB bump (red thick line). Only stars without close companions of comparable or brighter

luminosity have been selected, in order to avoid stellar contamination within the fibers.

All the spectra have been reduced with the standard ESO GIRAFFE pipeline<sup>2</sup>, including bias-subtraction, flat-fielding, wavelength calibration with a reference Th-Ar lamp and extraction of the 1-dimensional spectra.

Radial velocities (RVs) have been measured for each individual spectrum from the position of several metallic lines using the code DAOSPEC (Stetson & Pancino 2008). After the correction for the corresponding heliocentric velocity, the spectra of each star have been coadded together and used for the chemical analysis. Typical SNR per pixel are 70-100 for HR12, 120-150 for HR13 and 180-230 for HR15N.

We excluded from the following chemical analysis 6 stars with RV not compatible with that of Omega Centauri and 4 stars with RV dispersion larger than 1.7 km/s (while all the other targets have RV dispersions significantly smaller than 1 km/s) and considered as candidate binary stars. Finally, we derived chemical abundances for a total of 201 member stars of Omega Centauri. All the main information (coordinates, magnitudes, RVs) of the member stars are listed in Table 1.

### 3. Chemical analysis

Effective temperatures ( $T_{\text{eff}}$ ) and surface gravities ( $\log g$ ) have been derived from the photometric information.  $T_{\text{eff}}$  have been obtained by averaging  $T_{\text{eff}}$  derived from  $(B - V)_0$ ,  $(V - I)_0$  and  $(V - K_s)_0$  from the Alonso, Arribas & Martinez-Roger (1999) transformations.  $B$ ,  $V$  and  $I$  magnitudes are from Bellini et al. (2009),  $K_s$  magnitude from 2MASS database (Skrutskie et al. 2006). Because the Alonso, Arribas & Martinez-Roger (1999) calibration adopted the Johnson I-filter, the Cousin I-band magnitudes by Bellini et al. (2009) have been transformed to the Johnson photometric system adopting the transformation provided by Bessell (1979). The  $K_s$  2MASS magnitudes have been transformed to the Telescopio Carlos Sanchez photometric system (used by Alonso, Arribas & Martinez-Roger 1999) by means of the relations by Carpenter (2001) and Alonso, Arribas & Martinez-Roger (1998).

The dereddened colours have been obtained by adopting the extinction coefficients from McCall (2004) and the colour excess quoted in the Harris (1996, 2010 edition) catalogue ( $E(B - V) = 0.12$  mag). Note that Omega Centauri is not significantly affected by differential reddening (Bellini et al. 2009) and this effect has been neglected in the atmospheric parameters determination,

2MASS  $K_s$  magnitudes are available for 143 stars and for them we averaged the three  $T_{\text{eff}}$  values. For 54 stars we used only  $T_{\text{eff}}$  derived from  $(B - V)_0$  and  $(V - I)_0$ , and for 4 stars (for which  $I$  and  $K_s$  magnitudes are not available)  $T_{\text{eff}}$  from  $(B - V)_0$  have been adopted. We checked that no significant offset exists among the different  $T_{\text{eff}}$  scales: the average differences between the  $T_{\text{eff}}$  scales are  $T_{\text{eff}}^{(V-K_s)} - T_{\text{eff}}^{(B-V)} = +49$  K ( $\sigma = +74$  K),  $T_{\text{eff}}^{(V-K_s)} - T_{\text{eff}}^{(V-I)} = +45$  K ( $\sigma = +51$  K) and  $T_{\text{eff}}^{(B-V)} - T_{\text{eff}}^{(V-I)} = -30$  K ( $\sigma = +61$  K).

Gravities have been derived through the Stefan-Boltzmann relation, adopting the photometric  $T_{\text{eff}}$  described above, a true distance modulus of  $(m - M)_0 = 13.70$  mag (Bellazzini et al. 2004), the bolometric corrections calculated according to Alonso, Arribas & Martinez-Roger (1999), while the evolutive mass have been estimated according to a grid of theoretical

isochrones of different metallicities from the BaSTI database (Pietrinferni et al. 2006).

Microturbulent velocities ( $v_t$ ) have been derived spectroscopically by erasing any trend between the line strength and the iron abundance using  $\sim 35$ -40 Fe I lines.

Chemical abundances for Fe and Al have been derived with the code GALA (Mucciarelli et al. 2013)<sup>3</sup> by comparing the theoretical and measured equivalent widths (EWs) of unblended metallic lines. The adopted model atmospheres have been calculated with the last version of the code ATLAS9<sup>4</sup> (see Sbordone et al. 2004; Kurucz 2005). EWs have been measured with the code DAOSPEC (Stetson & Pancino 2008) managed through the wrapper 4DAO (Mucciarelli 2013)<sup>5</sup>. For some stars, Al lines are too weak to be measured and we computed upper limits adopting as EW 3 times the uncertainty calculated according to the Cayrel (1988) formula.

Abundances for Li and Na have been derived through a  $\chi^2$ -minimization, performed with our own code SALVADOR, between the observed and synthetic spectra. The synthetic spectra have been computed with the code SYNTHE (Sbordone et al. 2004; Kurucz 2005), including all the atomic and molecular transitions from the Kurucz/Castelli linelist. The Li abundances have been derived from the Li resonance doublet at  $\sim 6708$  Å, including the corrections for non-local thermodynamical equilibrium from Lind et al. (2008). Lithium abundances have been derived for 168 targets, while for 33 stars the Li line is too weak and only upper limits are provided. Na abundances from the Na D doublet at 5890-5896 Å have been corrected for departures from local thermodynamical equilibrium adopting the corrections computed by Lind et al. (2011).

Abundance uncertainties have been calculated by adding in quadrature the errors arising from the measurement procedure (EW or spectral fitting) and those arising from the adopted atmospheric parameters (uncertainties in  $T_{\text{eff}}$  and  $\log g$  have been added directly because the two parameters are correlated). For Fe and Al, we consider as internal error the dispersion normalized to the root mean square of the number of used lines. For Li and Na abundances, derived from spectral synthesis, we estimated the uncertainties in the fitting procedure resorting to MonteCarlo simulations. For each star, a sample of 300 noisy spectra has been created, injecting Poissonian noise in the best-fit synthetic spectrum (rebinning to the FLAMES-GIRAFFE pixel-size). Each sample of spectra has been analysed with the same procedure adopted for the real spectra. The dispersion of the derived abundance distribution has been assumed as  $1\sigma$  uncertainty in the abundance. Uncertainties due to the atmospheric parameters have been derived by repeating the analysis varying each time one only parameter by the corresponding uncertainty ( $\sigma_{T_{\text{eff}}} = \pm 50$  K,  $\sigma_{v_t} = \pm 0.1$  km s<sup>-1</sup>,  $\sigma_{\log g} = \pm 0.1$ ).

Typical formal uncertainties in  $A(\text{Li})$  are of the order of 0.05-0.07 dex, being the uncertainty in  $T_{\text{eff}}$  the dominant source of error for these abundances, while the error due to the fitting procedure is smaller than 0.03 dex, because of the high SNR of the spectra. Atmospheric parameters, abundance ratios and their uncertainties for all the member stars are listed in Table 2.

### 4. [Fe/H] distribution

Fig. 2 shows the [Fe/H] distribution of the entire sample (upper panel) as a generalized histogram (a representation that removes

<sup>3</sup> <http://www.cosmic-lab.eu/gala/gala.php>

<sup>4</sup> <http://www.user.oats.inaf.it/castelli/sources/atlas9codes.html>

<sup>5</sup> <http://www.cosmic-lab.eu/4dao/4dao.php>

<sup>2</sup> <http://www.eso.org/sci/software/pipelines/>

**Table 1.** Main information on the member LRGB targets of Omega Centauri. Coordinates and B, V, I magnitudes are from Bellini et al. (2009),  $K_s$  magnitudes are 2MASS database (Skrutskie et al. 2006). This table is available in its entirety in machine-readable form.

ID	RA (J2000)	Dec (J2000)	B	V	I	$K_s$	$RV_{\text{hel}}$ ( $\text{km s}^{-1}$ )
22580	201.723137	-47.661730	15.630	14.747	13.660	12.293	+216.2±0.2
25939	201.832739	-47.653890	15.818	14.950	13.874	12.394	+227.8±0.1
31135	201.784629	-47.643055	15.707	14.843	13.760	12.370	+239.0±0.1
35536	201.750357	-47.634749	15.634	14.763	13.677	12.269	+224.8±0.1
45849	201.765455	-47.617715	15.616	14.762	13.752	12.461	+252.3±0.1
49844	201.735347	-47.611785	15.890	14.981	13.868	12.450	+223.9±0.1
56555	201.683982	-47.602406	16.002	15.053	13.948	12.548	+218.5±0.1
57780	201.709221	-47.600836	15.972	15.041	13.951	12.592	+224.0±0.2
64366	201.683249	-47.592755	15.904	15.013	13.914	12.460	+224.6±0.2
67162	201.724149	-47.589388	15.880	14.976	13.897	12.504	+245.2±0.1
70485	201.812966	-47.585439	15.568	14.723	13.644	12.303	+237.4±0.1
71476	201.601550	-47.584175	15.551	14.699	13.641	12.246	+227.1±0.2
73028	201.820008	-47.582544	15.665	14.787	13.706	12.339	+233.3±0.1
73743	201.920362	-47.581721	15.851	14.985	13.907	12.533	+253.1±0.1
73986	201.741336	-47.581473	15.683	14.787	13.692	12.197	+259.6±0.1
74878	201.892105	-47.580466	15.712	14.846	13.764	12.419	+243.7±0.1
77093	201.563334	-47.578011	15.792	14.919	13.832	12.487	+222.1±0.2

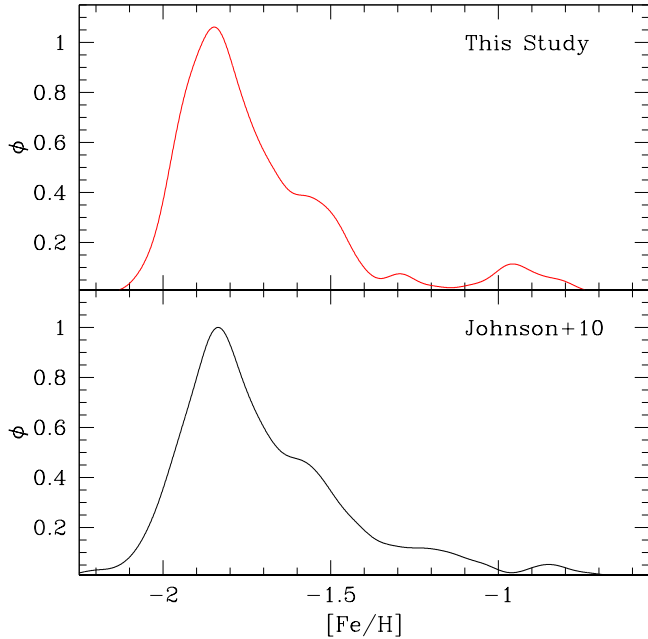


**Fig. 2.** Generalized histograms for the LRGB stars of Omega Centauri discussed in this study (upper panel) and for the bright RGB stars discussed by Johnson & Pilachowski (2010), shifted by  $-0.08$  dex in order to match the main peaks of the two distributions.

the effects due to the choice of the starting point and of the bin size, by taking into account the uncertainties in each individual value, see Laird et al. 1988).

The iron distribution ranges from  $-2.06$  dex to  $-0.76$  dex, with a main peak at  $[\text{Fe}/\text{H}] \sim -1.85$  dex, a clear second peak at  $[\text{Fe}/\text{H}] \sim -1.55$  dex and a long metal-rich tail with a clump of stars at  $[\text{Fe}/\text{H}] \sim -0.9$  dex and a possible small peak at  $[\text{Fe}/\text{H}] \sim -1.3$  dex. This distribution is qualitatively similar to those previously discussed in other studies (Johnson et al.

2008, 2009; Johnson & Pilachowski 2010; Marino et al. 2011). The lower panel of Fig. 2 shows the  $[\text{Fe}/\text{H}]$  distribution by Johnson & Pilachowski (2010) that presented the largest (855 stars) dataset of abundances for RGB stars of Omega Centauri. We note that the main peak of our distribution is slightly most metal-poor than that by Johnson & Pilachowski (2010). We estimate a difference of  $-0.08$  dex between the median values of the metal-poor components of the two distributions. In Fig. 2 the  $[\text{Fe}/\text{H}]$  distribution by Johnson & Pilachowski (2010) has been shifted by  $-0.08$  dex in order to match the main peaks of the two distributions. Because there are no stars in common with this study (that is focussed on RGB stars brighter than the RGB bump) we cannot directly investigate the origin of this small difference. However, we noted that the V-band magnitudes used by Johnson & Pilachowski (2010) are brighter than those of Bellini et al. (2009) by about 0.1 mag (while the  $K_s$ -band magnitudes are the same), leading to slightly hotter  $T_{\text{eff}}$  with respect to our ones. Despite this small offset, the two distributions are very similar.

Following the scheme used by Johnson & Pilachowski (2010) to describe their  $[\text{Fe}/\text{H}]$  distribution, we adopted the nomenclature proposed by Sollima et al. (2005a) to associate the individual RGBs observed in the CMD of Omega Centauri with the components of its iron distribution. The main peak in our  $[\text{Fe}/\text{H}]$  distribution can be associated to the RGB-MP (the main giant branch observed in the CMD of Omega Centauri), the second peak to the RGB-Int1, while the most metal-rich peak to the anomalous RGB. Sollima et al. (2005a) identified other two RGBs, with metallicities intermediate between those of RGB-Int1 and the anomalous RGB. Johnson & Pilachowski (2010) identified the stars in the range  $[\text{Fe}/\text{H}] \sim -1.4/-1.0$  dex in their  $[\text{Fe}/\text{H}]$  distribution as belonging to the RGB-Int2 and RGB-Int3. In our distribution this  $[\text{Fe}/\text{H}]$  range is less populated with respect to the Johnson & Pilachowski (2010) distribution, probably because of a poor sampling of the reddest stars (our targets are confined to a narrow strip on the CMD, see Fig. 1).

**Table 2.** Atmospheric parameters and abundance ratios (and corresponding uncertainties) for the member LRGB stars in Omega Centauri. This table is available in its entirety in machine-readable form.

ID	$T_{\text{eff}}$ (K)	log g	$v_t$ (km s <sup>-1</sup> )	[Fe/H]	A(Li) <sub>NLTE</sub>	[Na/Fe] <sub>NLTE</sub>	[Al/Fe]
22580	4901	2.31	1.5	-1.98±0.07	1.02±0.05	-0.42±0.08	<0.94
25939	4890	2.39	1.6	-1.71±0.07	1.00±0.05	-0.26±0.07	<0.45
31135	4913	2.36	1.3	-1.78±0.07	0.85±0.05	+0.18±0.06	<0.57
35536	4907	2.33	1.5	-1.60±0.07	0.71±0.06	+0.31±0.07	+1.29±0.08
45849	5068	2.41	1.6	-1.49±0.07	<0.67	+0.16±0.08	<0.27
49844	4848	2.38	1.7	-1.67±0.07	1.03±0.07	-0.25±0.07	<0.49
56555	4843	2.41	1.6	-1.65±0.07	0.90±0.05	+0.20±0.05	+0.51±0.10
57780	4879	2.41	1.3	-1.87±0.07	0.91±0.05	-0.15±0.07	<0.77
64366	4857	2.41	1.4	-1.77±0.07	0.90±0.06	-0.20±0.05	<0.50
67162	4899	2.41	1.4	-1.54±0.07	0.78±0.06	+0.39±0.05	+1.39±0.07
70485	4943	2.32	1.5	-1.86±0.07	0.84±0.05	+0.13±0.07	+1.09±0.08
71476	4944	2.31	1.6	-1.80±0.07	0.82±0.05	+0.09±0.07	+1.10±0.07
73028	4930	2.35	1.5	-1.49±0.07	0.72±0.05	+0.39±0.05	+1.37±0.05
73743	4921	2.41	1.3	-1.84±0.07	1.08±0.06	+0.09±0.05	<0.72
73986	4852	2.31	1.4	-1.58±0.07	0.81±0.05	+0.24±0.06	+1.43±0.08
74878	4927	2.36	1.5	-1.81±0.07	1.02±0.06	+0.07±0.07	<0.59
77093	4918	2.38	1.4	-1.85±0.09	1.04±0.07	-0.29±0.09	<0.77

## 5. Lithium in Omega Centauri

We discuss here the A(Li) distribution in 199 LRGB stars of Omega Centauri, excluding two targets that reveal a high Li content and that will be discussed in a forthcoming paper.

The upper panel of Fig. 3 shows the behaviour of A(Li) as a function of [Fe/H] for the true measures (166 stars, grey circles) and the upper limits (33 stars, red arrows). Considering only the true measures, the A(Li) distribution ranges from 0.47 to 1.19 dex. The A(Li) distribution clearly peaks at A(Li)~1 dex but with the presence of a significant fraction of stars with A(Li)<0.8 dex. Stars with A(Li)~1 dex are found only at [Fe/H]<-1.3 dex, while Li-poor stars are found at all the metallicities. In particular, the A(Li) distribution for stars with [Fe/H]<-1.6 dex (corresponding to the main population of Omega Centauri, RGB-MP) is dominated by stars with A(Li)~1 dex. In the [Fe/H] range between -1.6 and -1.3 dex (likely connected to RGB-Int1) the distribution is dominated by stars with A(Li)<0.8 dex, while the component at A(Li)~1 dex decreases in number. For [Fe/H]>-1.3 dex the component with A(Li)~1 dex totally disappears and all stars have A(Li) lower than ~0.6–0.7 dex.

The lower panel of Fig. 3 shows the run of the ratio between the number of Li-rich and Li-poor stars (defined assuming A(Li)= 0.8 dex as threshold) as a function of the iron abundance. The data have been grouped in 4 metallicity bins, chosen according to the metallicity distribution (Fig. 2), centred at [Fe/H]= -1.85, -1.55, -1.30 and -0.9 dex, and with width of 0.45, 0.20, 0.34 and 0.3 dex. The stars with [Fe/H]<-1.65 dex show a constant number ratio that drops at higher metallicity, reaching 0 for the most metal-rich stars where all the stars have A(Li)<0.8.

In order to assess whether the lack of Li-rich stars in the metal-rich regime is real or due to small number statistics, we performed a MonteCarlo simulation from a A(Li) distribution resembling that observed for stars with [Fe/H]<-1.6 dex. We extracted from this distribution 10,000 samples of 40 stars and 10,000 samples of 15 stars, corresponding to the number of stars observed in the third and fourth metallicity bin, respectively. We found that the probability to observe a  $N_{\text{Li-rich}}/N_{\text{Li-poor}}$  number ratio smaller than 0.5 is 0 and less than 0.03% for the two samples, ruling out that the observed lack of stars with A(Li)~1 dex is due to the small number of stars. Also, we checked that dif-

ferent choices for the metallicity bins do not change this conclusion. Hence, the difference between the A(Li) distributions of metal-poor and metal-rich stars is real.

The peak of the number distribution of A(Li) for the metal-poor stars well agrees with the A(Li) abundances previously measured in Population II LRGB stars, i.e. in Milky Way field stars (Mucciarelli, Salaris & Bonifacio 2012), in Galactic GCs (Lind et al. 2009; Mucciarelli et al. 2011; D’Orazi et al. 2014, 2015) and in the extra-galactic GC M54 (Mucciarelli et al. 2014). This finding confirms the previous result (based on dwarf stars) by Monaco et al. (2010) that Omega Centauri formed with the same lithium content of other Population II stars, formed in the Milky Way. Considering only the stars with [Fe/H]<-1.3 dex, the main peak of the A(Li) number distribution (A(Li)>0.8 dex) includes about 60% of the stars. This fraction well matches the fraction of the true measures of A(Li) among dwarf stars of Omega Centauri analysed by Monaco et al. (2010) in a similar range of metallicity ([Fe/H]<-1.4 dex).

The most interesting feature in this A(Li) distribution is the lack of stars with A(Li)~1 dex at metallicities higher than [Fe/H]~-1.3 dex. The blue line shown in Fig. 3 is the expected run of A(Li) with [Fe/H] in LRGB stars assuming that they are all born with the same initial A(Li), according to models from Mucciarelli, Salaris & Bonifacio (2012) and assuming an age of 12.5 Gyr. In particular, we assumed an initial value able to match the observed A(Li) of the peak of the number distribution of the metal-poor component; however the shape of the curve is independent of the assumed value for the initial A(Li). The model predicts that A(Li) in LRGB stars mildly decreases over a large range of [Fe/H] and only for [Fe/H]>-0.9 dex should rapidly drop due to the deeper convective envelope of such metal-rich stars. If we assume that all the stars in Omega Centauri formed with the same initial Li content, a clear drop of the Li abundance is expected at [Fe/H]>-0.9/-0.8 dex. Instead, the stars of Omega Centauri with [Fe/H]>-1.3 dex are systematically depleted in lithium. We recall that LRGB stars of GCs with [Fe/H]~-1.1/-1.2 dex (see e.g. M4, Mucciarelli et al. (2011); Monaco et al. (2012) and NGC 2808, D’Orazi et al. 2015) have A(Li) compatible with that measured in metal-poor clusters.

We investigated if other parameters can affect the behaviour of A(Li) in these stars, in particular the helium mass fraction

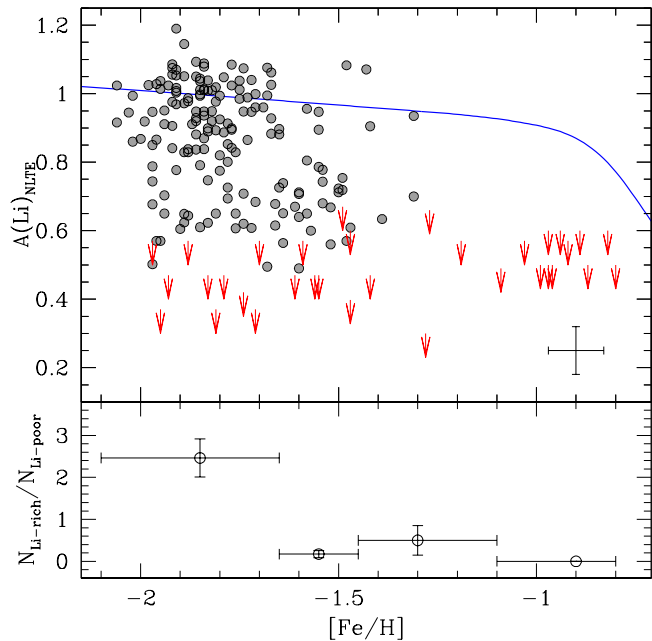


**Fig. 3.** Upper panel: behaviour of  $A(\text{Li})$  as a function of  $[\text{Fe}/\text{H}]$  (grey points are the true measures, red arrows mark the upper limits). The blue line shows the theoretical behaviour of  $A(\text{Li})$  as a function of  $[\text{Fe}/\text{H}]$  in LRGB stars starting from the same initial  $A(\text{Li})$ . Lower panel: behaviour of the fraction of number of stars with  $A(\text{Li}) > 0.8$  and with  $A(\text{Li}) < 0.8$  as a function of  $[\text{Fe}/\text{H}]$  computed for four metallicity bins. Vertical error-bars represent the uncertainties in the number ratio, the horizontal error-bars denote the corresponding metallicity range.

$Y$  and the stellar age. Several photometric observations (like the extended blue horizontal branch and the splitting of the main sequence) reveal a large spread in the initial He content of Omega Centauri stars. In particular, the most metal-rich populations have been suggested to have a helium mass fraction up to  $Y \sim 0.35$  (Norris 2004; Piotto et al. 2005; Sollima et al. 2005b; Renzini 2008). We checked that for metallicity  $[\text{M}/\text{H}] = -1.01$  dex, an increase of  $Y$  from 0.24 up to 0.35 changes the value of  $A(\text{Li})$  in LRGB stars by only 0.03 dex.

The precise age spread in Omega Centauri is still debated and the metal-rich populations are proposed to be coeval to the main population or significantly younger by some Gyr (see e.g. Ferraro et al. 2004; Freyhammer et al. 2005; Villanova et al. 2014; Tailo et al. 2016). However, a decrease of the age from 12.5 Gyr to 8.5 Gyr (both adopting  $Y = 0.25$  and  $Y = 0.35$ ) leads to a decrease of  $A(\text{Li})$  by  $\sim 0.05$ – $0.06$  dex with respect to the value calculated for 12.5 Gyr and  $Y = 0.25$ . Therefore, an increase of the He content and/or a decrease of the age cannot explain the drop of  $A(\text{Li})$  observed for  $[\text{Fe}/\text{H}] > -1.3$  dex.

Finally, we note that the model predictions for the surface  $A(\text{Li})$  of the observed RGB stars (blue line in Figure 3) do include potential surface Li depletion during the MS, due to burning at the bottom of the convective envelopes.

## 6. Li-Na anti-correlation

The comparison between Li and Na abundances provides important clues to understand the nature of the Li-poor stars observed at all the metallicities in Omega Centauri. This stellar system has

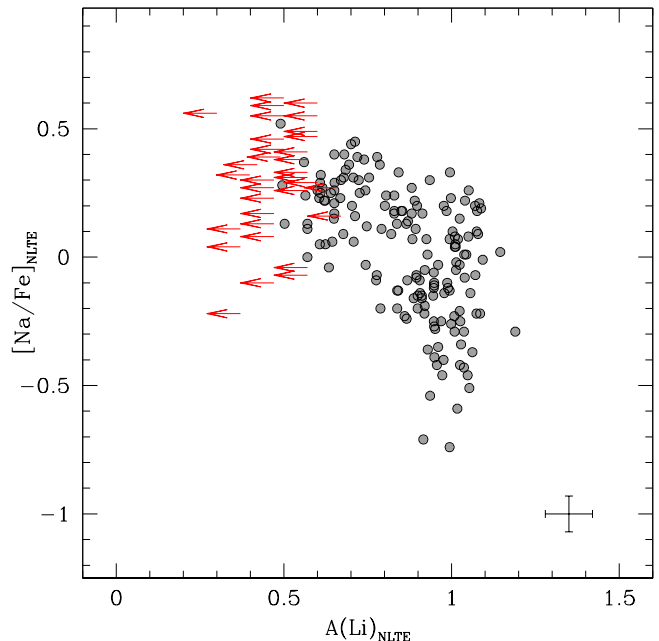


**Fig. 4.** Behaviour of  $[\text{Na}/\text{Fe}]$  as a function of  $A(\text{Li})$  for the entire spectroscopic sample studied in this work (grey circles). Red arrows mark the upper limits for  $A(\text{Li})$ .

a wide range of  $[\text{Na}/\text{Fe}]$ , from  $[\text{Na}/\text{Fe}] \sim -0.5$  dex to  $\sim +0.6$  dex. Note that our  $[\text{Na}/\text{Fe}]$  distribution is shifted toward lower values with respect to those measured by Johnson & Pilachowski (2010) and Marino et al. (2011), because these two works do not take into account departures from the local thermodynamical equilibrium (the corrections for the Na abundances are usually negative). Fig. 4 and Fig. 5 show the run of  $[\text{Na}/\text{Fe}]$  and  $[\text{Al}/\text{Fe}]$  as a function of  $A(\text{Li})$ , respectively. Red arrows mark the upper limits for Li, blue arrows the upper limits for  $[\text{Al}/\text{Fe}]$ . In both plots a clear anti-correlation is found, with the stars with the higher  $A(\text{Li})$  covering a large range of  $[\text{Na}/\text{Fe}]$  and  $[\text{Al}/\text{Fe}]$ , while the stars with  $A(\text{Li})$  lower than  $\sim 0.8$  dex have systematically higher  $[\text{Na}/\text{Fe}]$  and  $[\text{Al}/\text{Fe}]$  abundances. A direct evidence of this behaviour is shown in Fig. 6, where the spectra of two stars with similar atmospheric parameters and metallicity are compared (namely #206770 and #213229, red and black curves respectively). As clearly visible, the spectrum of #213229 shows Al and Na lines stronger than those of #206770 (where the Al lines are totally lacking) but also an undetectable Li line, clearly visible in the other spectrum.

The Li-Na anticorrelation is visible only in the metal-poor stars, because the presence of a significant star-to-star  $A(\text{Li})$  scatter is restricted to  $[\text{Fe}/\text{H}] < -1.3$  dex (see Fig. 3). In particular, the stars with low  $A(\text{Li})$  are all significantly enriched in Na, even if other stars with similar high Na have normal  $A(\text{Li})$ . Fig. 7 shows the behaviour of  $[\text{Na}/\text{Fe}]$  as a function of  $[\text{Fe}/\text{H}]$  for our sample (a similar run has been found also by Johnson & Pilachowski 2010; Marino et al. 2011).  $[\text{Na}/\text{Fe}]$  increases with the iron content and the higher Na abundances are measured in the most metal-rich stars. Hence, stars with  $[\text{Fe}/\text{H}] > -1.3$  dex are all depleted in Li but enriched in Na.

We compare the Li-Na distribution of Omega Centauri with those measured in mono-metallic GCs, namely NGC 6397, NGC 6752, M4 and 47 Tucanae. The distributions of Li-Na of these clusters are shown in Fig. 8 in comparison with that of

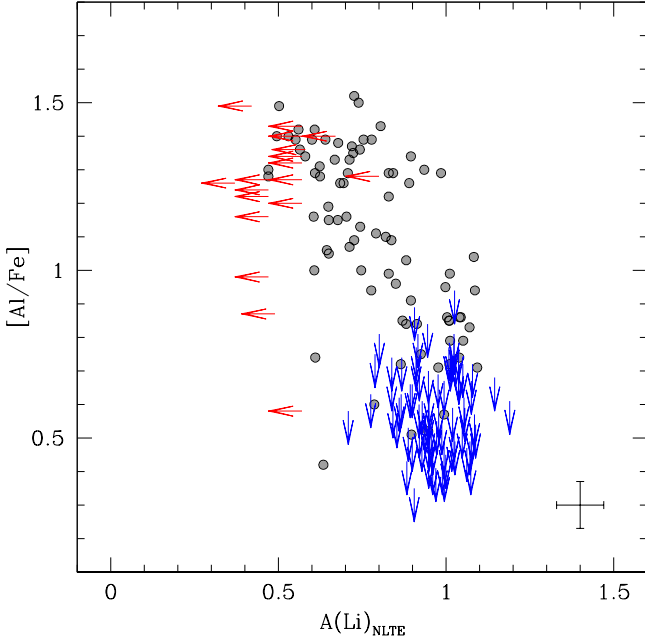


**Fig. 5.** Behaviour of  $[Al/Fe]$  as a function of  $A(Li)$  for the entire spectroscopic sample studied in this work (grey circles). Red arrows mark the upper limits for  $A(Li)$ , blue arrows the upper limits for  $Al$ .

the LRGB stars in Omega Centauri: light grey points/arrows is the entire sample of target stars studied here, while dark grey points/arrows show the target stars of Omega Centauri selected with metallicities close to that of the comparison GCs included in each panel. Because the  $Li$  abundances in these GCs are measured in dwarf stars we shifted them in order to match the median  $A(Li)$  of each cluster with the peak of the  $A(Li)$  distribution of Omega Centauri (that is lower due to the effect of the FDU).

In NGC 6397 (blue circles in Fig. 8) most of the 100 dwarf stars studied by Lind et al. (2009) have a similar  $A(Li)$  but over a large range of  $Na$  (hence corresponding to 1P and 2P stars). Among these 100 targets, three stars have  $A(Li)$  lower than the other stars by  $\sim 0.4$ – $0.5$  dex and they have the highest values of  $[Na/Fe]$  of the sample.

NGC 6752 (green circles) shows a clear  $Li$ - $Na$  anticorrelation (Pasquini et al. 2005) where the most  $Li$ -poor stars have  $A(Li)$  lower by  $\sim 0.4$  dex with respect to the most  $Li$ -rich stars. At variance with NGC 6397 (and also Omega Centauri) where most of the stars exhibit a large  $Na$  spread but similar  $A(Li)$ , in NGC 6752 the  $Na$  and  $Li$  abundances in the studied stars follow a linear behaviour. Even if the sample discussed by Pasquini et al. (2005) includes only 9 dwarf stars, its large spread in  $A(Li)$  has been confirmed by Shen et al. (2010) with a sample of 112 dwarf stars (and where a  $Li$ - $O$  correlation has been detected).

Monaco et al. (2012) present  $Na$  and  $Li$  abundances in 70 dwarf stars in M4 (red triangles in Fig. 8), excluding one  $Li$ -rich star. The  $Na$ - $Li$  distribution in M4 is similar to that of NGC 6397, with most of the stars with similar  $Li$  content and different  $[Na/Fe]$  but a larger star-to-star scatter in  $A(Li)$  among the 2P stars. Note that the most  $Li$ -poor star in this sample has a  $A(Li)$  lower by  $\sim 0.3$  dex than the median  $A(Li)$  value and it is among the most  $Na$ -rich stars.

47Tucanae (cyan squares in Fig. 8) exhibits a large star-to-star scatter in its  $Li$  content. D’Orazi et al. (2010) and

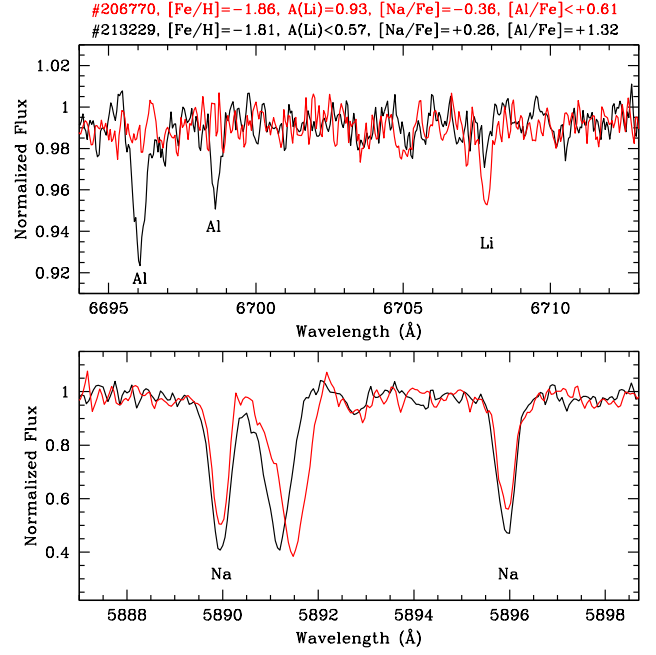


**Fig. 6.** Comparison between two stars of Omega Centauri, namely #206770 and #213229 (red and black curves respectively), with similar atmospheric parameters and metallicity but different depths for  $Li$ ,  $Na$  and  $Al$  lines. The two strong lines at  $\sim 5891$  Å visible in the lower panel and shifted each other are  $Na$  interstellar lines.

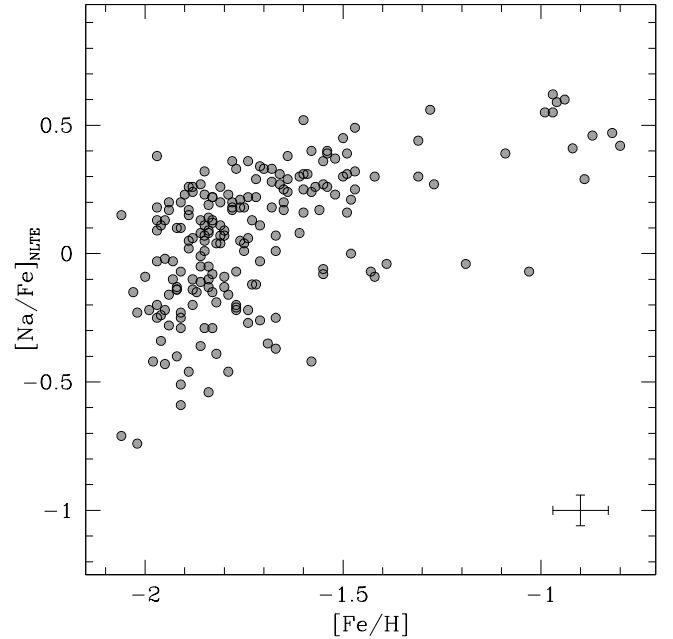


**Fig. 7.** Behaviour of  $[Na/Fe]$  as a function of  $[Fe/H]$ .

Dobrovolskas et al. (2014) from the analysis of 110 dwarf stars in this cluster do not find clear evidence of  $Li$ - $Na$  anticorrelation, while a hint of  $Li$ - $O$  correlation is detected.

Other GCs have been investigated by D’Orazi et al. (2014, 2015) that discuss the behaviour of  $A(Li)$  in LRGB stars as a function of  $Al$  abundance. In most of these GCs (namely

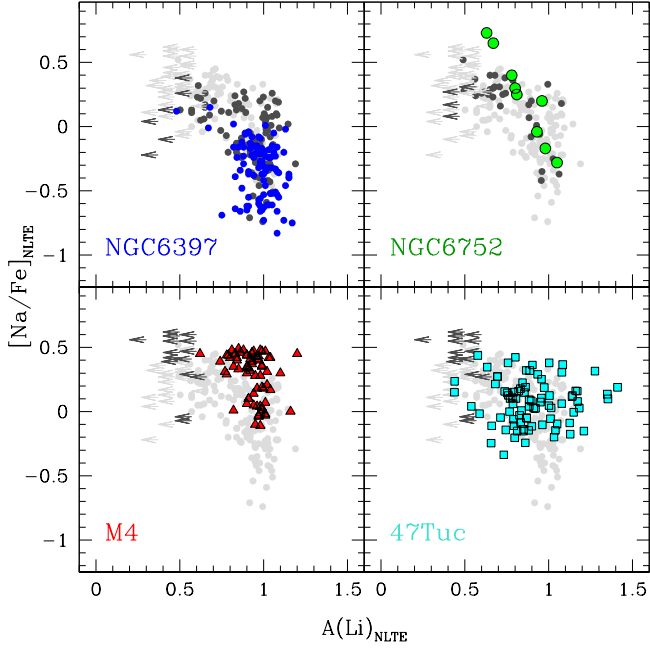


**Fig. 8.** Comparison between the  $[\text{Na}/\text{Fe}]$ - $A(\text{Li})$  distribution of the stars in Omega Centauri (grey points and arrows) and the abundances measured in dwarf stars of some mono-metallic GCs from the literature, namely NGC 6397 (blue circles, Lind et al. 2009), NGC 6752 (green circles, Pasquini et al. 2005), M4 (red triangles, Monaco et al. 2012) and 47 Tucanae (cyan squares, Dobrovolskas et al. 2014). The  $A(\text{Li})$  abundances in these four clusters have been lowered in order to match their median value with the  $A(\text{Li})$  measured in LRGB stars of Omega Centauri. Light grey points/arrows indicate the entire sample of stars in Omega Centauri studied here, dark grey points/arrows are the target stars selected with a metallicity similar to that of the reference Galactic GC shown in each panel.

NGC 362, NGC 1904, NGC 5904 and NGC 6218) all the stars have the same  $A(\text{Li})$  regardless of the  $A(\text{Li})$  abundance. On the other hand, in NGC 2808 some Al-rich LRGB stars have  $A(\text{Li})$  lower by  $\sim 0.3$  dex than that in other stars with similar Al content.

## 7. Summary and conclusions

We derived surface lithium abundances for 199 LRGB stars members of the stellar system Omega Centauri and distributed over its entire metallicity range. The main results are:

- the  $A(\text{Li})$  number distribution of LRGB stars in Omega Centauri is peaked at  $A(\text{Li}) \sim 1$  dex, compatible with the abundances measured in LRGB stars belonging to other GCs and in metal poor field stars and this abundance can be considered as the normal  $A(\text{Li})$  in Population II LRGB stars. Additionally, the  $A(\text{Li})$  distribution of Omega Centauri shows also a prominent Li-poor tail ( $A(\text{Li}) \leq 0.8$  dex);
- the stars with normal  $A(\text{Li})$  are found at  $[\text{Fe}/\text{H}] < -1.3$  dex, while the Li-poor stars are found at all the metallicities. All the stars with  $[\text{Fe}/\text{H}] > -1.3$  dex exhibit low  $A(\text{Li})$  values;
- a clear Li-Na anticorrelation is found. The stars with normal  $A(\text{Li})$  cover a large range of  $[\text{Na}/\text{Fe}]$ , with  $A(\text{Li}) \leq 0.8$  dex are characterized by enhanced values of  $[\text{Na}/\text{Fe}]$ . Similarly, a Li-Al anticorrelation is detected.

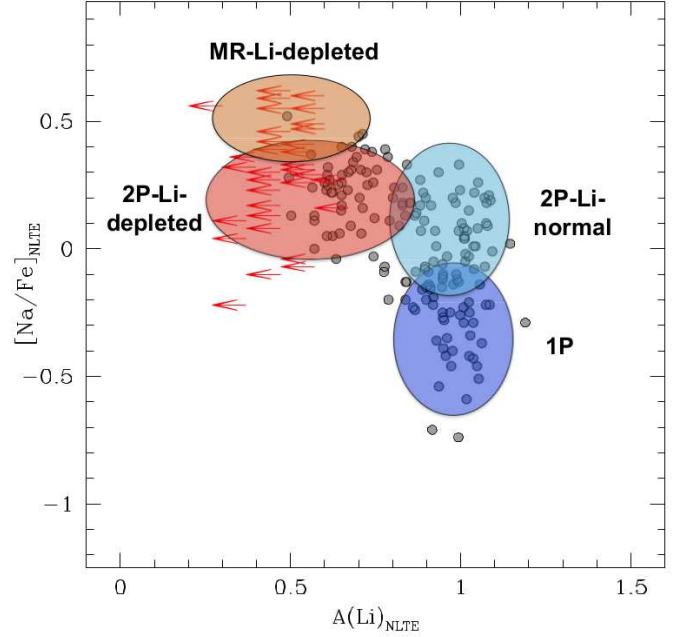


**Fig. 9.** Same of Fig. 4 but with super-imposed the mean loci for the proposed classification of the Omega Centauri's stars according to their Li and Na abundances.

The  $A(\text{Li})$  distribution in Omega Centauri is more complex than those observed in mono-metallic GCs, reflecting the peculiar (and not yet totally understood) chemical evolution of this system. We can draw a qualitative scheme to describe this distribution, classifying the stars according to their, Li, Na and Fe abundances. In particular,  $[\text{Na}/\text{Fe}]$  has been used to discriminate between 1P (low  $[\text{Na}/\text{Fe}]$ ) and 2P (high  $[\text{Na}/\text{Fe}]$ ) stars. We identify four main groups of stars, sketched in Fig. 9:

1. 1P stars ( $[\text{Fe}/\text{H}] < -1.3$  dex), with low  $[\text{Na}/\text{Fe}]$  and normal Li.
2. 2P stars ( $[\text{Fe}/\text{H}] < -1.3$  dex) enriched in  $[\text{Na}/\text{Fe}]$  and with the same (normal)  $A(\text{Li})$  measured in 1P stars; hereafter we refer to these stars as *2P-Li-normal*
3. 2P stars ( $[\text{Fe}/\text{H}] < -1.3$  dex) enriched in  $[\text{Na}/\text{Fe}]$  like the *2P-Li-normal* stars but depleted Li ( $A(\text{Li}) \leq 0.8$  dex) and here named *2P-Li-depleted*;
4. Stars with  $[\text{Fe}/\text{H}] > -1.3$  dex (labelled as *MR-Li-depleted*) that have  $A(\text{Li}) \leq 0.6$  dex and high  $[\text{Na}/\text{Fe}]$  abundances. In particular, the  $[\text{Na}/\text{Fe}]$  abundance of these stars is slightly higher than that of 2P stars, because the  $[\text{Na}/\text{Fe}]$  increases with the metallicity (see Fig. 7 and also Johnson & Pilachowski 2010; Marino et al. 2011).

The classification proposed in Fig. 9 provides only a simple guideline to highlight the complexity of the Li-Na distribution in this system, and the main features to be explained by models for the formation of Omega Centauri. It does not imply a specific formation timeline.

The overall picture is that mono-metallic GCs (see Fig. 8) show, to a lesser extent, the same sub-populations identified in the metal-poor stars of Omega Centauri. These clusters are dominated by 1P and *2P-Li-normal* stars, with the presence of a minor component of Na-rich, Li-poor stars (even if the identification of a clear boundary between *2P-Li-normal* and *2P-Li-depleted* populations is not trivial). On the other hand, the fraction of *2P-Li-depleted* stars observed in Omega Centauri ( $\sim 30\%$ )

turns out to be exceptional with respect to the other GCs, where the fraction of these stars is about 3-5%.

Within the canonical views of the formation of multiple populations, 1P stars would correspond to the first stellar generation and we can consider their surface A(Li) as a good tracer of the initial lithium content of the stellar system (after the effect of the FDU is taken into account). The high [Na/Fe] measured in the other (2P) stars indicates that these stars formed from a gas enriched by the products of proton-capture cycles (occurring at temperatures higher than that of Li-burning). The timeline of the formation of the 2P stars (both with normal and depleted Li content) in Omega Centauri depends on the chemical evolution of the system and on the role played by the different polluter stars. The 2P-Li-depleted stars may have formed from a Li-poor or Li-free gas (diluted with pristine gas) coming from fast-rotating massive stars that are not able to produce fresh Li (Decressin et al. 2007). On the other hand, the high A(Li) measured among the 2P-Li-normal stars suggests a production of new Li. Massive AGB stars are potentially able to produce Li through the Cameron-Fowler mechanism and they may explain the Li abundance in most of the Na-rich stars.

However, theoretical models for A(Li) in GCs based on AGB stars as main polluters depend on several parameters, in particular the yields of the AGB models (the production of Li in these stars is sensitive to the stellar mass) and the lithium abundance of the pristine material (see D'Antona et al. 2012, for a discussion on these assumptions). D'Antona et al. (2012) discussed for M4 the case of polluters ejecta that are Li-free (a case similar to that of fast-rotating massive stars) and diluted with pristine gas, finding only a mildly lower (by about 0.1 dex) A(Li) in 2P stars with respect to 1P stars. Hence, high A(Li) in Na-rich stars could be explained also with polluter stars not able to produce fresh Li, depending on the details of the dilution process. The need of some fine-tuning to reproduce the uniform Li content observed in stars with a large spread in Na abundance, as well as uncertainties in the theoretical mass-loss rates and Li yields, reduce the predictive power of these models.

Another peculiarity of Omega Centauri is the low Li abundance in its metal-rich stars. The stars with  $[Fe/H] > -1.3$  dex exhibit an unexpected depletion of A(Li), not observed in GCs with comparable metallicities (i.e. M4 and NGC 2808) that show in most of their (dwarf or LRGB) stars A(Li) similar to that measured in metal-poor clusters. We demonstrated that the effect of high metallicity, high He content and/or young age (that could characterize the high-metallicity stars in Omega Centauri) cannot explain the observed values, under the assumption that all the stars of Omega Centauri formed with the same initial A(Li). Hence, we conclude that the *MR-Li-depleted* stars formed from a gas already depleted in A(Li) (similar to the *2P-Li-depleted* stars) and the observed Li depletion is not an effect of the FDU. According to this finding, we should observe in the metal-rich main sequence stars of Omega Centauri a surface A(Li) smaller than the typical value of the *Spite Plateau*. The observation of these stars is very challenging due to their faintness. Monaco et al. (2010) and Pancino et al. (2011b) provide upper limits for A(Li) in 18 stars belonging to the metal-rich sub-giant branch of Omega Centauri. Unfortunately, the upper limits for the initial Li content of these stars do not provide conclusive answers.

An additional hurdle with respect to mono-metallic GCs is the possible age spread of the stellar populations of Omega Centauri. There is no general consensus about the relative ages of the different stellar components of the system, in particular between the main (metal-poor) population and the most metal-

rich one that could be virtually coeval (see e.g. Tailo et al. 2016) or several Gyr younger (see e.g. Villanova et al. 2014). If the metallicity enrichment of Omega Centauri took place on short timescales (in particular if the metal-rich stars are coeval or only slightly younger than the other populations), the most metal-rich stars have formed before other sources of Li production occur, like novae and cosmic rays spallation (see e.g. Romano et al. 1999).

Detailed theoretical models for the Li-Na behaviour in Omega Centauri are not available so far. In particular, future theoretical models for Omega Centauri need to simultaneously explain: (i) the existence of stars with similar A(Li) but different [Na/Fe] (1P and *2P-Li-normal*); (ii) the existence of stars with similar [Na/Fe] but different A(Li) (*2P-LiR* and *2P-Li-depleted*); (iii) the *MR-Li-depleted* component, with the lowest A(Li) and the highest [Na/Fe].

The discussed set of abundances will be crucial to put new constraints to the chemical enrichment history of this stellar system.

*Acknowledgements.* The authors thank the anonymous referee for his/her useful comments and suggestions. SV gratefully acknowledges the support provided by Fondecyt reg. n. 1170518. LM acknowledges the support from "Proyecto interno" of the Universidad Andres Bello. AM warmly thanks Federico Montaguti and Olma for their essential support during the last year.

## References

- Alonso, A., Arribas, S., & Martinez-Roger, C., 1998, *A&As*, 131, 209  
 Alonso, A., Arribas, S., & Martinez-Roger, C., 1999, *A&As*, 140, 261  
 Bastian, N., & Lardo, C., 2015, *MNRAS*, 453, 357  
 Bastian, N., & Lardo, C., 2017, arXiv171201286  
 Bedin, L. R., Piotto, G., Anderson, J., Cassisi, S., King, I. R., Moman, Y., & Carraro, G., 2004, *ApJ*, 605L, 125  
 Bellazzini, M., Ferraro, F. R., Sollima, A., Pancino, E., & Origlia, L., 2004, *A&A*, 424, 199  
 Bellini et al., 2009, *A&A*, 493, 958  
 Bekki, K., & Freeman, K. C., 2003, *MNRAS*, 346, L11  
 Bessell, M. S., 1979, *PASP*, 91, 589  
 Bonifacio, P., 2002, *A&A*, 390, 91  
 Cayrel, R., 1988, in *IAU Symposium*, Vo. 132, The Impact of very high S/N spectroscopy on stellar physics, ed. G. Cayrel de Strobel & M. Spite, 345  
 Carpenter, J. M., 2001, *AJ*, 121, 2851  
 Carretta, E., Bragaglia, A., Gratton, R., et al., 2009, *A&A*, 505, 117  
 Carretta, E., Bragaglia, A., Gratton, R., & Lucatello, S., 2009, *A&A*, 505, 139  
 Carretta, E., Bragaglia, A., Gratton, R., D'Orazi, V., & Lucatello, S., 2009, *A&A*, 508, 695  
 D'Antona, F., D'Ercole, A., Carini, R., Vesperini, E., & Ventura, P., 2012, *MNRAS*, 426, 1710  
 Decressin, T., Charbonnel, C., & Meynet, G., 2007, *A&A*, 475,  
 Dekker, H., D'Odorico, S., Kaufer, A., Delabre, B., & Kotzlowski, H., 2000, *SPIE*, 4008, 534  
 D'Ercole, A., Vesperini, E., D'Antona, F., McMillan, S. L. W., & Recchi, S., 2008, *MNRAS*, 391, 825  
 D'Ercole, A., D'Antona, F., Ventura, P., Vesperini, E., & McMillan, S. L. W., 2010, *MNRAS*, 407, 854  
 Dobrovolskas, V., et al., 2014, *A&A*, 565, 121  
 D'Orazi, V., Lucatello, S., Gratton, R., Bragaglia, A., Carretta, E., Shen, Z., & Zaggia, S., 2010, *ApJ*, 713L, 1  
 D'Orazi, V. & Marino, A. F., 2010, *ApJ*, 716L, 166  
 D'Orazi, V., Angelou, G. C., Gratton, R. G., Lattanzio, J. C., Bragaglia, A., Carretta, E., Lucatello, S., & Momany, Y., 2014, *ApJ*, 791, 39  
 D'Orazi, V., Gratton, R. G., Angelou, G. C., Bragaglia, A., Carretta, E., Lattanzio, J. C., Lucatello, S., Momany, Y., Sollima, A., & Beccari, G., 2015, *MNRAS*, 449, 4038  
 Ferraro, F. R., Sollima, A., Pancino, E., Bellazzini, M., Straniero, O., Origlia, L. & Cool, A. M., 2004, *ApJ*, 603L, 81  
 Freyhammer, L. M. et al., 2005, *ApJ*, 623, 860  
 Gonzalez Hernandez, J. I., Bonifacio, P., Caffau, E., Steffen, M., Ludwig, H.-G., Behara, N. T., Sbordone, L., Cayrel, R., & Zaggia, S., 2009, *A&A*, 505L, 13  
 Gratton, R. G., Carretta, E., & Bragaglia, A., 2012, *A&ARv*, 20, 50

- Johnson, C., O., Pilachowski, C. A., Simmerer, J., & Schwenk, D., 2008, *ApJ*, 681, 1505
- Johnson, C., O., Pilachowski, C. A., Michael, R. R., & Fulbright, J. P., 2009, *ApJ*, 698, 2048
- Johnson, C. L., & Pilachowski, C. A., 2010, *ApJ*, 722, 1373
- Harris, W.E. 1996, *AJ*, 112, 1487
- Kraft, R. P., Sneden, C., Langer, G. E., & Prosser, C. F., 1992, *AJ*, 104, 645
- Kurucz, R. L., 2005, *MSAIS*, 8, 14
- Laird, J. B., Rupen, M. P., Carney, B. W. & Latham, D. W., 1988, 96, 1908L
- Lee, Y.-W., Joo, J.-M., Sohn, Y.-J., Rey, S.-C., Lee, H.-C., & Walker, A. R., 1999, *Nature*, 402, 55
- Lind, K., Asplund, M., Barklem, P. S., & Belyaev, A. K., 2008, *A&A*, 528, 103
- Lind, K., Primas, F., Charbonnel, C., Grundahl, F., & Asplund, M., 2009, *A&A*, 503, 545
- Lind, K., Asplund, M., Barklem, P. S., & Belyaev, A. K., 2011, *A&A*, 528, 103
- Marino, A. F. et al., 2011, *ApJ*, 731, 64
- McCall, M. L., 2004, *AJ*, 128, 2144
- Meynet, G., Ekström, S. & Maeder, A., 2006, *A&A*, 447, 623
- Meszáros, S. et al., 2015, *AJ*, 149, 153
- Milone, A. P. et al., 2008, *ApJ*, 673, 241
- Monaco, L., Bonifacio, P., Sbordone, L., Villanova, S., & Pancino, E., 2010, *A&A*, 519L, 3
- Monaco, L., Villanova, S., Bonifacio, P., Caffau, E., Geisler, D., Marconi, G., Monary, Y., & Ludwig, H.-G., 2012, *A&A*, 539, 157
- Mucciarelli, A., Salaris, M., Lovisi, L., Ferraro, F. R., Lanzoni, B., Lucatello, S. & Gratton, R. G. 2011, *MNRAS*, 412, 81
- Mucciarelli, A., Salaris, M., & Bonifacio, P., 2012, *MNRAS*, 419, 2195
- Mucciarelli, A., Pancino, E., Lovisi, L., Ferraro, F. R., & Lapenna, E., 2013, *ApJ*, 766, 78
- Mucciarelli, A., 2013, arXiv1311.1403
- Mucciarelli, A., Salaris, M., Bonifacio, P., Monaco, L. & Villanova, S., 2014, *MNRAS*, 444, 1812
- Norris, J. E., 2004, *ApJ*, 612, L25
- Pancino, E., Ferraro, F. R., Bellazzini, M., Piotto, G., & Zoccali, M., 2000, *ApJ*, 534L, 83
- Pancino, E., Mucciarelli, A., Sbordone, L., Bellazzini, M., Pasquini, L., Monaco, L. & Ferraro, F. R., 2011, *A&A*, 527, 18
- Pancino, E., Mucciarelli, A., Bonifacio, P., Monaco, L., & Sbordone, L., 2011, *A&A*, 534, 53
- Pancino, E., et al., 2017, *A&A*, 601, 112
- Pasquini, L., et al., 2000, *SPIE*, 4008, 129
- Pasquini, L., Bonifacio, P., Molaro, P., Francois, P., Spite, F., Gratton, R. G., Carretta, E., & Wolf, B., 2005, *A&A*, 441, 549
- Pietrinferni, A., Cassisi, S., Salaris, M., & Castelli, F., 2006, *ApJ*, 642, 797
- Piotto, G. et al., 2005, *ApJ*, 621, 777
- Prantzos, N. & Charbonnel, C., 2006, *A&A*, 458, 135
- Renzini, A., 2008, *MNRAS*, 391, 354
- Renzini, A., D'Antona, F., Cassisi, S., et al., 2015, *MNRAS*, 454, 4197
- Romano, D., Matteucci, F., Molaro, P., & Bonifacio, P., 1999, *A&A*, 352, 117
- Sbordone, L., Bonifacio, P., Castelli, F. & Kurucz, R. L., 2004, *MSAIS*, 5, 93
- Shen, Z.-X., Bonifacio, P., Pasquini, L., & Zaggia, S., 2010, *A&A* 524L, 2
- Skrutskie, M. F., et al., 2006, *AJ*, 131, 1163
- Smith, G. H. & Norris, J., 1982, *ApJ*, 254, 149
- Sollima, A., Ferraro, F. R., Pancino, E. & Bellazzini, M., 2005, *MNRAS*, 357, 265
- Sollima, A., Pancino, E., Ferraro, F. R., Bellazzini, M., Straniero, O. & Pasquini, L., 2005, *ApJ*, 634, 332
- Sollima, A., Ferraro, F. R., Bellazzini, M., Origlia, L., Straniero, O., & Pancino, E., 2007, *ApJ*, 654, 915
- Stetson, P. B., & Pancino, E., *PASP*, 120, 1332 K. 2005, *PASP*, 57, 27
- Tailo, M., Di Criscienzo, M., D'Antona, F., Caloi, V., & Ventura, P., 2016, *MNRAS*, 457, 4525
- Ventura, P., D'Antona, F., Mazzitelli, I. & Gratton, R. G., 2001, *ApJ*, 550L, 65
- Villanova, S., Geisler, D., Gratton, R. G., & Cassisi, S., 2014, *ApJ*, 791, 107
- Willman, B., & Strader, J., 2012, *AJ*, 144, 76